

# Efficient Generation of Two-Photon Excited Phosphorescence from Molecules in Plasmonic Nanocavities

Oluwafemi S. Ojambati, Rohit Chikkaraddy, William M. Deacon, Junyang Huang, Demelza Wright, and Jeremy J. Baumberg\*



Cite This: <https://dx.doi.org/10.1021/acs.nanolett.0c01593>



Read Online

ACCESS |



Metrics & More



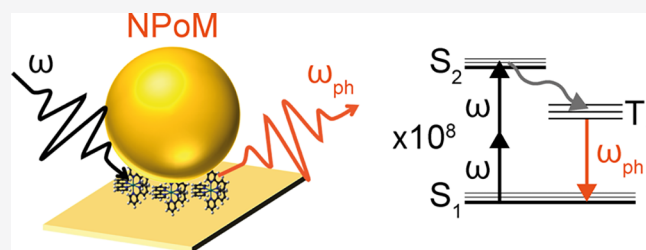
Article Recommendations



Supporting Information

**ABSTRACT:** Nonlinear molecular interactions with optical fields produce intriguing optical phenomena and applications ranging from color generation to biomedical imaging and sensing. The nonlinear cross-section of dielectric materials is low and therefore for effective utilisation, the optical fields need to be amplified. Here, we demonstrate that two-photon absorption can be enhanced by  $10^8$  inside individual plasmonic nanocavities containing emitters sandwiched between a gold nanoparticle and a gold film. This enhancement results from the high field strengths confined in the nanogap, thus enhancing nonlinear interactions with the emitters. We further investigate the parameters that determine the enhancement including the cavity spectral position and excitation wavelength. Moreover, the Purcell effect drastically reduces the emission lifetime from 520 ns to <200 ps, turning inefficient phosphorescent emitters into an ultrafast light source. Our results provide an understanding of enhanced two-photon-excited emission, allowing for optimization of efficient nonlinear light-matter interactions at the nanoscale.

**KEYWORDS:** nanocavity, plasmonic enhancement, phosphorescence, two-photon absorption, Purcell factor



Nonlinear optics is widely used for the generation of different laser colors, spectroscopy, imaging, optical communications, light modulation devices, and more.<sup>1–7</sup> Due to the weak nonlinearities of transparent materials, nonlinear light–matter interactions require high optical intensities and typically demand pulsed lasers<sup>1</sup> or resonant cavities.<sup>8</sup> The intensity requirement limits their otherwise promising application for probing nanodevices, whose subdiffraction-limited active regions provide faint signals unless high power densities are used that almost inevitably damage the nanostructures.<sup>9,10</sup>

The solution demonstrated here is to employ closely spaced metallic nanostructures that support coherent collective electron oscillations within localized plasmons.<sup>11</sup> Plasmonic nanostructures have been used to enhance fluorescence emission,<sup>12–16</sup> surface-enhanced Raman spectroscopy,<sup>17–20</sup> and nonlinear light generation.<sup>21–25</sup> There has been growing interest in using plasmonic nanostructures to enhance two-photon excited emission where photons with half the energy of an electronic transition, typically in the near-infrared (NIR), excite an emitter which then emits in the visible region.<sup>26</sup> Such two-photon excitation has been used for deep tissue penetration,<sup>27,28</sup> since both elastic scattering and absorption are reduced at NIR wavelengths. Moreover, two photon absorption has been widely used for optical power limiting,<sup>29</sup> optical communications,<sup>30</sup> and single photon nonlinear detectors.<sup>31</sup>

Plasmon enhancement of this two-photon excitation should yield much larger enhancements compared to one-photon excitation, due to the quadratic dependence of emission on local excitation intensity. However, plasmonic nanostructures have so far given two-photon enhancements ranging only from one to four orders of magnitude.<sup>32–35</sup> The emission depends on the enhanced optical electric field  $E$  in the vicinity of the probed emitter which varies with nanostructure geometry and is maximized for coupled plasmons trapped between two metallic nanocomponents (e.g., dimers<sup>33</sup>) or at the sharp ends of metallic nanostructures (e.g., nanorods<sup>32</sup>). To go beyond these previous studies and realize the potential for nano-nonlinearities, we exploit the extreme confinement recently accessed in sub-nm plasmonic gaps.

Drastically enhanced two-photon-excited emission is obtained from the nanoparticle-on-mirror (NPoM) construct used here, which consists of a Au nanoparticle sitting on top of a monolayer molecular emitter [here, tris(2,2'-bipyridine) ruthenium(II) hexafluorophosphate, known as “Rubpy”, see [Methods](#)] assembled on a flat gold film ([Figure 1a](#)). Plasmonic

**Received:** April 13, 2020

**Revised:** May 14, 2020

**Published:** May 18, 2020



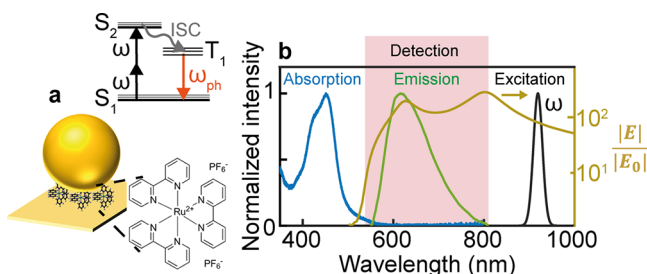


**Figure 1.** Experimental scheme. (a) Plasmonic nanocavity formed by a Au nanoparticle on a Au film with Rubpy in the gap. The inset shows the chemical structure of the Rubpy emitter and its energy levels excited from the ground singlet state  $S_0$  to the first excited singlet  $S_1$  via two-photon absorption of near-infrared light. The emitter undergoes ultrafast intersystem crossing (ISC) to the triplet  $T_1$  and phosphoresces in the visible wavelength region. (b) Absorption (blue) and emission (green) spectra of Rubpy in solution, with near-field enhancement (brown) calculated for an 80 nm Au nanoparticle with a 20 nm facet width. The NPoM is excited by 120 fs pulses at 920 nm (black). The red-shaded region is the detection window.

modes equivalent to the prototypical plasmon dimer are confined between the nanoparticle and the Au mirror.<sup>36–38</sup> The long wavelength coupled plasmon mode position confirms that only a molecular monolayer sits in the  $\sim 1$  nm gap (Methods), which results in field enhancements that exceed 280 (see Figure 1b), so that strong two-photon excited emission is expected. The Rubpy chromophore used here is a widely studied phosphorescent emitter that absorbs in the ultraviolet (around 450 nm) and has a large Stokes shift with a phosphorescence peak at 620 nm (Figure 1b). This broad emission couples to the NPoM cavity which possesses a fundamental resonance in the near-infrared. Rubpy has a relatively high nonlinear absorption cross-section, up to  $180.10^{-50} \text{ cm}^4 \text{ photon}^{-1} \text{ s}^{-1}$ .<sup>39,40</sup>

## RESULTS

**Two-Photon Excitation.** We perform two-photon excitation from  $S_0$  to  $S_1$  on Rubpy in NPoMs, and compare to in solution. A 920 nm pump laser with 120 fs pulses elicits phosphorescent emission between 550 and 800 nm (Figure 1b). The emission spectra for increasing excitation powers (Figure 2a,b) show minimal changes in spectral shape but strong differences between NPoM and 80  $\mu\text{M}$  Rubpy solution. The darkfield scattering, which reveals the NPoM cavity mode, remains constant even up to 1 mW average power on the NPoM (Figure 2c), which implies that the NPoM nanoconstruct is stable with no significant damage or migration of Au atoms.<sup>41,42</sup> To understand the difference between Rubpy emission from NPoMs and in solution, it is sufficient to account for in-/out-coupling efficiencies using a simple analytical model based on the darkfield scattering multiplied by the solution spectra (Figures 2d, described below). The NPoMs thus simply filter the Rubpy emission spectrum through their fundamental mode.

**Emission Enhancement.** To further understand how NPoMs modify the emission, the integrated intensity across the emission spectra is extracted for each excitation power. In both NPoMs and in solution, the integrated intensities scale quadratically with power density (Figure 3a), confirming that two-photon absorption drives the observed emission. This behavior persists in all component parts of the spectrum

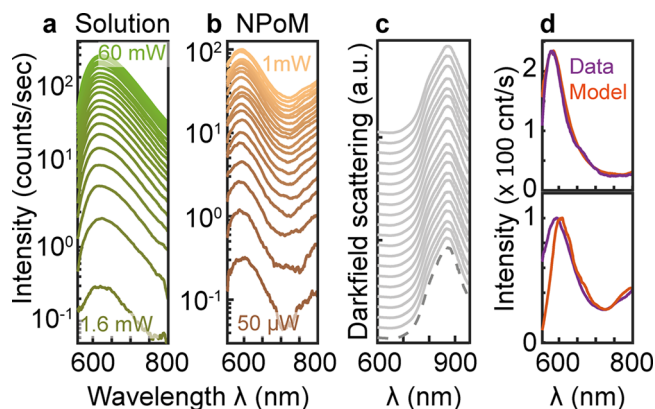


**Figure 2.** Emission and scattering spectra. Phosphorescence spectra of Rubpy (a) in solution and (b) in a nanoparticle-on-mirror (NPoM) nanocavity. (c) Darkfield scattering spectra of the NPoM after each laser illumination, vertically offset for clarity. The dashed line in (c) is the initial darkfield. (d) Emission and modeled spectra of two different NPoMs.

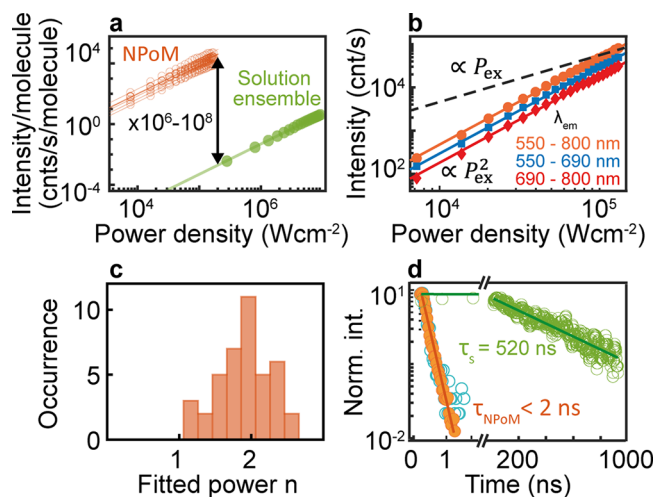


**Figure 3.** Power dependence of emission. (a) Measured emission per molecule integrated over all detected wavelengths vs power density, for seven different nanoparticle-on-mirror (NPoM) nanocavities with Rubpy spacers (orange) and in solution (green). Solid lines are power law fits with an exponent of two. (b) Intensity vs power density within different spectra regions (as noted). (c) Histogram of power law exponents obtained from power scaling in  $>40$  NPoM cavities. (d) Normalized intensity vs time delay from time-correlated single-photon counting of emission from bulk Rubpy (green open circles), Rubpy in NPoM (orange filled circles), and instrument response function measured with attenuated laser pulses (cyan open circles).

(Figure 3b), showing that they originate from the same state. Analyzing results on more than 40 NPoM cavities shows that the quadratic scaling dominates with variations between powers of 1.6 to 2.3 (Figure 3c). We estimate the experimental enhancement factor per molecule of Rubpy, in NPoMs with respect to in solution, as

$$EF_e = \frac{I_N}{I_s} \times \frac{N_s}{N_N} \times \frac{C_s}{C_N} \quad (1)$$

where  $I_N$  and  $I_s$  are the measured integrated intensity (in counts/seconds/ $\mu\text{W}$ ) across the detection wavelength range in NPoM (N) and in solution (s), respectively,  $N_{N,s}$  are the numbers of molecules, and  $C_{N,s}$  are the collection efficiencies

to account for the differences in radiation patterns of emitters in NPoM and in solution (for the estimation of these parameters and detailed description of the enhancement calculation, see SI Note 2, and for error analysis, see SI Note 3). We estimate  $N_N$  using the measured surface coverage of Rubpy on Au<sup>43</sup> and the calculated area of the hotspot at the center of the gap which is set by the lateral mode  $I^2(r)$  profile (since via two-photon absorption) of which 50% is within a radius of 4.7 nm. Similarly  $N_s$  uses the 80  $\mu\text{M}$  solution concentration and illuminated volume set by the focused spot size  $w_0$  of 0.51  $\mu\text{m}$  (at  $\lambda = 0.92$ , numerical aperture NA = 0.9) and Rayleigh length  $z_R$  of 0.9  $\mu\text{m}$ . The collection  $C_s = 0.67$  comes from Lambertian emission with 5% losses and the solid angle restricted by total internal reflection at the glass–air interface, while  $C_N = 0.55$  is given by the predominantly high angle emission of the NPoM collected by the same NA = 0.9 objective.<sup>44,45</sup>

Using eq 1, up to  $10^8$  emission enhancement from NPoMs is obtained compared to in solution. This strong enhancement results from the high field confinement in the nanocavity, thereby enhancing the two-photon absorption of the excitation light. We note that other methods can be used to determine the enhancement factor such as considering the ratio of the illuminated areas or volumes rather than the ratio of the number of molecules (for a discussion on this, see SI Note 2). Using the ratio of illuminated areas gives similar results (within a factor of 4, see Table S1) with  $N_{s,N}$ , while using the volume ratio gives erroneously high values (2 orders of magnitude higher), which is a result of the comparison of large volumes in solution with the small volume under the 1 nm NPoM gap. To avoid this exaggeration, we therefore use the estimated ratio of the number of molecules. In comparison with other nanophotonic structures used to enhance two-photon absorption, these NPoMs gives the highest enhancement (see Table 1).

**Table 1. Comparison of Two-Photon Excitation Enhanced by Different Nanostructures**

structure	two-photon enhancement	ref
nanocrystal/emitters coupled to surface plasmon	<10	35
perovskite-microcavity hybrid dielectric sphere	$10^2$	34
quantum dots in bowtie antennas	$10^3$	33
quantum dots near nanorods	$10^4$	32
emitters in NPoM	$10^6$ – $10^8$	present work

Below saturation, we determine the expected enhancement from simulation as

$$\text{EF}_s = \frac{\gamma_N \eta_N}{\gamma_s \eta_s} \sim 10^8 \quad (2)$$

where  $\gamma_N$  and  $\gamma_s$  are the excitation rates in NPoM and in solution, respectively, and  $\eta_{N,s}$  are the quantum yields (for further details, see SI Note 2). The ratio between experiments and simulations  $\frac{\text{EF}_e}{\text{EF}_s} = 0.01 - 1$  can be accounted for by less

controlled experimental parameters such as in-/out-coupling efficiencies of the NPoM, orientation, and spatial distribution of molecules in the gap.<sup>44</sup>

To demonstrate the Purcell effect, we measure the emission lifetime using time-correlated single-photon counting (TCSPC, see Methods) and obtain the lifetime for bulk Rubpy as  $\tau_{\text{bulk}} = 520 \pm 10$  ns and  $\tau_{\text{NPoM}} = 0.2 \pm 0.1$  ns, limited by the instrument response (Figure 3d). This implies that there is a >2600 emission speed-up due to the enhanced local density of optical states in the gap. From finite-difference time domain calculations, the Purcell factor is up to  $10^6$  (see Figure S4), and thus, a lifetime of  $\sim 500$  fs is expected, well below the detection speed of available single-photon counting modules.

**Dependence of emission on cavity resonance and excitation wavelength.** We investigate the dependence of the emission enhancement on the cavity resonance and observe that it is maximized when the plasmon peak matches the excitation wavelength (Figure 4a). This can be described using a model that assumes the total two-photon-absorbed in-coupled intensity  $I_a$  in the gap is

$$I_a = \int d\lambda [\sigma_a(\lambda)\eta(\lambda)I(\lambda_{\text{ex}})]^2 \sim [\sigma_a(\lambda_{\text{ex}})\eta(\lambda_{\text{ex}})I_{\text{ex}}]^2 \quad (3)$$

where the nonlinear absorption cross-section  $\sigma_a \propto \alpha(\lambda)$  tracks the linear absorption  $\alpha(\lambda)$  as established for Ru(II) complexes,<sup>46</sup>  $\eta$  is the in-coupling efficiency, and the excitation laser intensity is  $I$  for excitation wavelength  $\lambda_{\text{ex}}$ . For the in-coupling efficiency we take the darkfield scattering  $\eta \simeq S(\lambda)$ , which is modeled as the sum of two Lorentzian functions for each NPoM (Figure 4b) to model the plasmon transverse and cavity ( $\lambda_{\text{pk}}$ ) modes.<sup>45</sup> Taking the out-coupling efficiency also to be  $\eta$ , the total emitted intensity  $I_e = cN I_a \int_{\lambda_1}^{\lambda_2} d\lambda \eta(\lambda) I_s(\lambda)$

where  $c$  is a scaling factor,  $N$  is the number of molecules in the gap,  $I_s(\lambda)$  is the emission spectrum in solution, and  $\{\lambda_{1,2}\}$  is the detected emission wavelength range. The integrand of  $I_e$  well describes the spectral shape of the Rubpy emission spectra in

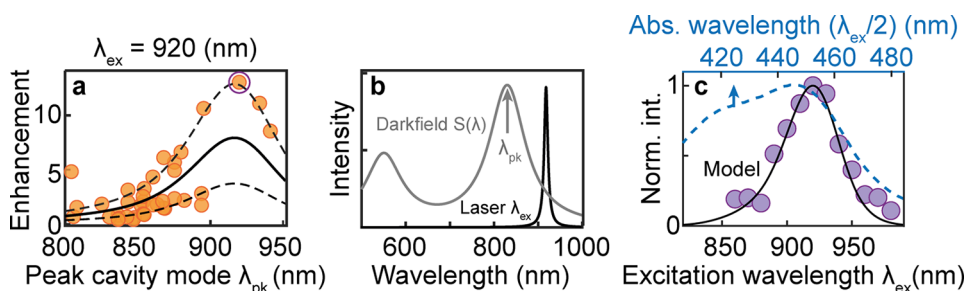


**Figure 4.** Emission dependence on cavity resonance and excitation wavelength. (a) Phosphorescence enhancement vs peak cavity mode for 43 NPoMs at  $\lambda_{\text{ex}} = 920$  nm (orange circles). Error bar is within the symbol size. Gray curves are analytical predictions for different scaling factors  $c$ . (b) Model darkfield spectra showing detuning of  $\lambda_{\text{ex}}$  from  $\lambda_{\text{pk}}$ . (c) Normalized emitted intensity vs excitation wavelength. Points are measured from a NPoM with peak  $\lambda$  indicated in the purple circle of Figure 4a,  $\alpha(\lambda_{\text{ex}}/2)$  is absorption spectrum of Rubpy at half the excitation wavelength (top axis).

NPoMs (Figure 2d). Defining  $\bar{\eta} = \int_{\lambda_1}^{\lambda_2} d\lambda \eta(\lambda) I_s(\lambda) / \int_{\lambda_1}^{\lambda_2} d\lambda I_s$  gives the normalized enhancement

$$G = \frac{I_e}{\int_{\lambda_1}^{\lambda_2} d\lambda I_s} = c\bar{\eta}NI_a \propto \bar{\eta}N[\alpha(\lambda_{ex})S(\lambda_{ex})]^2 \quad (4)$$

This model predicts that the emission is maximized when the cavity mode overlaps with the excitation wavelength, which agrees with our observations (Figure 4a). Different  $c$  factors can be attributed to a combination of variations in dipole orientation, molecular packing, diameter, and facet size of the Au nanoparticles.

Selecting now a NPoM with long-wavelength scattering peaks around 920 nm (giving the largest enhancements, but in the tail of the NPoM distribution, see Figure S1a), we vary the excitation wavelength and observe that the emission peaks when  $\lambda_{ex} = 920$  nm (Figure 4c). As expected, the spectral shape of this excitation curve depends on both the absorption spectrum at  $2\omega$  and the scattering resonance  $S(\lambda)$  near 920 nm. The strongest two-photon pumped emission occurs when there is a good overlap between the absorption spectrum, the excitation wavelength, and the plasmonic peak.

In summary, we employ plasmonic nanocavities to greatly enhance two-photon-excited emission by up to  $10^8$  and observe that the enhancement depends on tuning the excitation wavelength to both the nanocavity resonance and the molecular absorption. This enhancement, the highest yet reported, is due to the extreme field confinement producing thousand-fold intensity enhancement. Additional considerations to optimize two-photon yield are the position and dipole orientation of molecules in the NPoM gap, which is simplified here using monolayers of spherically symmetric Rubpy but can otherwise be challenging to control. Selective positioning and orienting can be achieved with DNA origami directed-assembly.<sup>47–50</sup> Superradiance and other cooperative effects are expected within the NPoM due to the small mode volume; however, we keep the occupancy per excitation low ( $<10^{-6}$  to reduce these effects).<sup>51–53</sup> Our results show that NPoMs are excellent nanophotonic constructs to explore nonlinear interactions at the nanoscale. These can open up applications in deep tissue biomedical imaging due to the enhanced emission (using similar NP dimers) as well as photodynamic therapy for efficient generation of singlet oxygen.<sup>54</sup>

## METHODS

**Optical Setup.** A detailed description of the experimental setup is in ref 55. We excite the sample with  $\sim 120$  fs pulses,  $\sim 10$  nm full width at half-maximum, generated from a tunable optical parametric oscillator (OPO) (Spectra Physics Inspire) pumped at 820 nm with a repetition rate of 80 MHz. The power of the pulses is controlled using a variable neutral density filter mounted on a rotational stage. The attenuated pulses pass through a 90:10 (reflection:transmission) beam splitter and are focused by a microscope objective with a numerical aperture = 0.9 to excite the emitters in the plasmonic nanocavity at high illumination angles ( $\leq 64^\circ$ ). Emission light passes through the beam splitter, through short pass filters, and is directed to a grating spectrometer using a removable mirror. The spectral image is also taken by an electron multiplying charged coupled detector (EMCCD) that is cooled to  $-80^\circ\text{C}$ . Taking out the removable mirror directs the emission light toward a time-correlated single-photon

counting (TCSPC) setup for the lifetime measurement which uses a single-photon avalanche photodiode (SPAD) and trigger SPAD. The output of the two SPADs are connected to a correlation card for histogramming.

**Sample Preparation.** First, 0.7 mg of tris(2,2'-bipyridine) ruthenium(II) hexa-fluorophosphate or Rubpy (Sigma-Aldrich) is dissolved in 10 mL of deionized water, and the solution is placed in an ultrasonic bath for 10 s to ensure proper dissolution. An atomically flat template-stripped Au on a Si wafer is submerged overnight in 1 mL of the Rubpy stock solution. The preparation of the template-stripped gold is described in ref 56. The substrate is thoroughly rinsed with deionized water and blown dry using nitrogen, leaving behind a self-assembled monolayer (SAM) of Rubpy on the Au film. Next, 200 mL of Au nanospheres (BBI Solutions, diameter 80 nm) that are stabilized in citrate buffer, mixed with a 5 mM of KCl solution (for further charge stabilization), is drop casted onto the Rubpy SAM on the Au substrate for 30 s. The excess Au nanoparticles solution is blown dry using nitrogen, and sparsely spaced Au nanoparticles are deposited on Rubpy on the Au film, forming the NPoM nanoconstruct. Characterization of the self-assembled structure using darkfield scattering spectroscopy reveals a dominant plasmonic mode with a peak at 830 nm (see Figure S1), indicating that the thickness of the nanogap is  $\sim 1$  nm, assuming a refractive index of 1.6, as predicted by a plasmonic circuit model and simulations.<sup>56,57</sup> A bilayer with a thickness of 2 nm would predict a darkfield scattering peak at 720 nm, far from the observed 830 nm peak, thus confirming that only a monolayer of Rubpy fits in the gap. The facet size ranges from 18–28 nm as seen in scanning electron microscope images of these nanoparticles,<sup>58</sup> and this is verified from the position of the quadrupole mode at 600 nm of the scattering spectrum (Figure S1). The surface coverage of a monolayer of Rubpy is estimated to be  $\sim 0.4 \times 10^{14}$  molecules  $\text{cm}^{-2}$  (see ref 43) to give  $\sim 30$  molecules (see SI) under each Au nanoparticle.

**Simulations.** Details of the simulations are provided in Supplementary Note 4.

## ■ ASSOCIATED CONTENT

### Supporting Information

The Supporting Information is available free of charge at <https://pubs.acs.org/doi/10.1021/acs.nanolett.0c01593>.

(Supplementary Note 1) Darkfield scattering and SERS, (Supplementary Note 2) enhancement calculation, (Supplementary Note 3) error analysis on the enhancement factor, and (Supplementary Note 4) finite-difference time domain (FDTD) simulations (PDF)

## ■ AUTHOR INFORMATION

### Corresponding Author

Jeremy J. Baumberg — NanoPhotonics Centre, Cavendish Laboratory, Department of Physics, JJ Thompson Avenue, University of Cambridge, Cambridge CB3 0HE, United Kingdom; [orcid.org/0000-0002-9606-9488](https://orcid.org/0000-0002-9606-9488); Email: [jjb12@cam.ac.uk](mailto:jjb12@cam.ac.uk)

### Authors

Oluwafemi S. Ojambati — NanoPhotonics Centre, Cavendish Laboratory, Department of Physics, JJ Thompson Avenue, University of Cambridge, Cambridge CB3 0HE, United Kingdom; [orcid.org/0000-0002-8028-4386](https://orcid.org/0000-0002-8028-4386)

**Rohit Chikkaraddy** – NanoPhotonics Centre, Cavendish Laboratory, Department of Physics, JJ Thompson Avenue, University of Cambridge, Cambridge CB3 0HE, United Kingdom; [orcid.org/0000-0002-3840-4188](https://orcid.org/0000-0002-3840-4188)

**William M. Deacon** – NanoPhotonics Centre, Cavendish Laboratory, Department of Physics, JJ Thompson Avenue, University of Cambridge, Cambridge CB3 0HE, United Kingdom

**Junyang Huang** – NanoPhotonics Centre, Cavendish Laboratory, Department of Physics, JJ Thompson Avenue, University of Cambridge, Cambridge CB3 0HE, United Kingdom

**Demelza Wright** – NanoPhotonics Centre, Cavendish Laboratory, Department of Physics, JJ Thompson Avenue, University of Cambridge, Cambridge CB3 0HE, United Kingdom

Complete contact information is available at:

<https://pubs.acs.org/10.1021/acs.nanolett.0c01593>

## Notes

The authors declare no competing financial interest.

Source data can be found at DOI link: <https://doi.org/10.17863/CAM.52531>.

## ACKNOWLEDGMENTS

We acknowledge funding from the EPSRC (Cambridge NanoDTC EP/L015978/1 and EP/S022953/1, EP/L027151/1, EP/P029426/1, and EP/N016920/1). O.S.O. acknowledges the support of Rubicon fellowship from the Netherlands Organisation for Scientific Research. R.C. acknowledges support from Trinity College, University of Cambridge.

## REFERENCES

- (1) Boyd, R. W. *Nonlinear Optics*; Elsevier: 2008.
- (2) Garmire, E. Nonlinear Optics in Daily Life. *Opt. Express* **2013**, *21* (25), 30532.
- (3) Dudley, J. M.; Genty, G.; Coen, S. Supercontinuum Generation in Photonic Crystal Fiber. *Rev. Mod. Phys.* **2006**, *78* (4), 1135–1184.
- (4) Zipfel, W. R.; Williams, R. M.; Webb, W. W. Nonlinear Magic: Multiphoton Microscopy in the Biosciences. *Nat. Biotechnol.* **2003**, *21* (11), 1369–1377.
- (5) Gu, B.; Zhao, C.; Baev, A.; Yong, K.-T.; Wen, S.; Prasad, P. N. Molecular Nonlinear Optics: Recent Advances and Applications. *Adv. Opt. Photonics* **2016**, *8* (2), 328.
- (6) Zhuang, L.; Roeloffzen, C. G. H.; Hoekman, M.; Boller, K.-J.; Lowery, A. J. Programmable Photonic Signal Processor Chip for Radiofrequency Applications. *Optica* **2015**, *2* (10), 854–859.
- (7) Ctistis, G.; Yuce, E.; Hartsuiker, A.; Claudon, J.; Bazin, M.; Gérard, J.-M.; Vos, W. L. Ultimate Fast Optical Switching of a Planar Microcavity in the Telecom Wavelength Range. *Appl. Phys. Lett.* **2011**, *98* (16), 161114.
- (8) Kavokin, A. V.; Baumberg, J. J.; Malpuech, G.; Laussy, F. P. Microcavities, 2nd ed.; *Series on Semiconductor Science and Technology*; Oxford University Press: Oxford, NY, 2017.
- (9) Chang, S.-S.; Shih, C.-W.; Chen, C.-D.; Lai, W.-C.; Wang, C. R. C. The Shape Transition of Gold Nanorods. *Langmuir* **1999**, *15* (3), 701–709.
- (10) Albrecht, W.; Deng, T.-S.; Goris, B.; van Huis, M. A.; Bals, S.; van Blaaderen, A. Single Particle Deformation and Analysis of Silica-Coated Gold Nanorods before and after Femtosecond Laser Pulse Excitation. *Nano Lett.* **2016**, *16* (3), 1818–1825.
- (11) Novotny, L.; Hecht, B. *Principles of Nano-Optics*; Cambridge University Press: 2006.
- (12) Barnes, W. L. Fluorescence near Interfaces: The Role of Photonic Mode Density. *J. Mod. Opt.* **1998**, *45* (4), 661–699.
- (13) Pelton, M. Modified Spontaneous Emission in Nanophotonic Structures. *Nat. Photonics* **2015**, *9* (7), 427–435.
- (14) Muskens, O. L.; Giannini, V.; Sánchez-Gil, J. A.; Gómez Rivas, J. Strong Enhancement of the Radiative Decay Rate of Emitters by Single Plasmonic Nanoantennas. *Nano Lett.* **2007**, *7* (9), 2871–2875.
- (15) Kinkhabwala, A.; Yu, Z.; Fan, S.; Avlasevich, Y.; Müllen, K.; Moerner, W. E. Large Single-Molecule Fluorescence Enhancements Produced by a Bowtie Nanoantenna. *Nat. Photonics* **2009**, *3* (11), 654–657.
- (16) Akselrod, G. M.; Argyropoulos, C.; Hoang, T. B.; Ciraci, C.; Fang, C.; Huang, J.; Smith, D. R.; Mikkelsen, M. H. Probing the Mechanisms of Large Purcell Enhancement in Plasmonic Nanoantennas. *Nat. Photonics* **2014**, *8* (11), 835–840.
- (17) Jeanmaire, D. L.; Van Duyne, R. P. Surface Raman Spectroelectrochemistry: Part I. Heterocyclic, Aromatic, and Aliphatic Amines Adsorbed on the Anodized Silver Electrode. *J. Electroanal. Chem. Interfacial Electrochem.* **1977**, *84* (1), 1–20.
- (18) Nie, S.; Emory, S. R. Probing Single Molecules and Single Nanoparticles by Surface-Enhanced Raman Scattering. *Science* **1997**, *275* (5303), 1102–1106.
- (19) Langer, J.; Jimenez de Aberasturi, D.; Aizpurua, J.; Alvarez-Puebla, R. A.; Auguie, B.; Baumberg, J. J.; Bazan, G. C.; Bell, S. E. J.; Boisen, A.; Brolo, A. G.; Choo, J.; Cialla-May, D.; Deckert, V.; Fabris, L.; Faulds, K.; García de Abajo, F. J.; Goodacre, R.; Graham, D.; Haes, A. J.; Haynes, C. L.; Huck, C.; Itoh, T.; Käll, M.; Kneipp, J.; Kotov, N. A.; Kuang, H.; Le Ru, E. C.; Lee, H. K.; Li, J.-F.; Ling, X. Y.; Maier, S.; Mayerhoefer, T.; Moskovits, M.; Murakoshi, K.; Nam, J.-M.; Nie, S.; Ozaki, Y.; Pastoriza-Santos, I.; Perez-Juste, J.; Popp, J.; Pucci, A.; Reich, S.; Ren, B.; Schatz, G. C.; Shegai, T.; Schlücker, S.; Tay, L. L.; Thomas, K. G.; Tian, Z.-Q.; Van Duyne, R. P.; Vo-Dinh, T.; Wang, Y.; Willets, K. A.; Xu, C.; Xu, H.; Xu, Y.; Yamamoto, Y. S.; Zhao, B.; Liz-Marzán, L. M. Present and Future of Surface Enhanced Raman Scattering. *ACS Nano* **2020**, *14* (1), 28–117.
- (20) Timmermans, F. J.; Lenferink, A. T. M.; van Wolferen, H. A. G. M.; Otto, C. Correlative SEM SERS for Quantitative Analysis of Dimer Nanoparticles. *Analyst* **2016**, *141* (23), 6455–6462.
- (21) Danckwerts, M.; Novotny, L. Optical Frequency Mixing at Coupled Gold Nanoparticles. *Phys. Rev. Lett.* **2007**, *98* (2), 1.
- (22) Ginzburg, P.; Orenstein, M. Nonlinear Effects in Plasmonic Systems. In *Active Plasmonics and Tuneable Plasmonic Metamaterials*; Zayats, A. V., Maier, S. A., Eds.; John Wiley & Sons, Inc.: Hoboken, NJ, USA, 2013; pp 41–67.
- (23) Butet, J.; Brevet, P.-F.; Martin, O. J. F. Optical Second Harmonic Generation in Plasmonic Nanostructures: From Fundamental Principles to Advanced Applications. *ACS Nano* **2015**, *9* (11), 10545–10562.
- (24) Genevet, P.; Tétienne, J.-P.; Gatzogiannis, E.; Blanchard, R.; Kats, M. A.; Scully, M. O.; Capasso, F. Large Enhancement of Nonlinear Optical Phenomena by Plasmonic Nanocavity Gratings. *Nano Lett.* **2010**, *10* (12), 4880–4883.
- (25) Ko, K. D.; Kumar, A.; Fung, K. H.; Ambekar, R.; Liu, G. L.; Fang, N. X.; Toussaint, K. C. Nonlinear Optical Response from Arrays of Au Bowtie Nanoantennas. *Nano Lett.* **2011**, *11* (1), 61–65.
- (26) Rumi, M.; Perry, J. W. Two-Photon Absorption: An Overview of Measurements and Principles. *Adv. Opt. Photonics* **2010**, *2* (4), 451.
- (27) Helmchen, F.; Denk, W. Deep Tissue Two-Photon Microscopy. *Nat. Methods* **2005**, *2* (12), 932.
- (28) Waterhouse, D. J.; Fitzpatrick, C. R. M.; Pogue, B. W.; O'Connor, J. P. B.; Bohndiek, S. E. A Roadmap for the Clinical Implementation of Optical-Imaging Biomarkers. *Nat. Biomed. Eng.* **2019**, *3* (5), 339–353.
- (29) Girardot, C.; Cao, B.; Mulatier, J.-C.; Baldeck, P. L.; Chauvin, J.; Riehl, D.; Delaire, J. A.; Andraud, C.; Lemerrier, G. Ruthenium(II) Complexes for Two-Photon Absorption-Based Optical Power Limiting. *ChemPhysChem* **2008**, *9* (11), 1531–1535.

- (30) Hayat, A.; Nevet, A.; Ginzburg, P.; Orenstein, M. Applications of Two-Photon Processes in Semiconductor Photonic Devices: Invited Review. *Semicond. Sci. Technol.* **2011**, *26* (8), 083001.
- (31) Boitier, F.; Dherbecourt, J.-B.; Godard, A.; Rosencher, E. Infrared Quantum Counting by Nondegenerate Two Photon Conductivity in GaAs. *Appl. Phys. Lett.* **2009**, *94* (8), 081112.
- (32) Zhang, W.; Caldarola, M.; Lu, X.; Orrit, M. Plasmonic Enhancement of Two-Photon-Excited Luminescence of Single Quantum Dots by Individual Gold Nanorods. *ACS Photonics* **2018**, *5* (7), 2960–2968.
- (33) Jensen, R. A.; Huang, I.-C.; Chen, O.; Choy, J. T.; Bischof, T. S.; Lončar, M.; Bawendi, M. G. Optical Trapping and Two-Photon Excitation of Colloidal Quantum Dots Using Bowtie Apertures. *ACS Photonics* **2016**, *3* (3), 423–427.
- (34) Liu, W.; Li, X.; Song, Y.; Zhang, C.; Han, X.; Long, H.; Wang, B.; Wang, K.; Lu, P. Cooperative Enhancement of Two-Photon-Absorption-Induced Photoluminescence from a 2D Perovskite-Microsphere Hybrid Dielectric Structure. *Adv. Funct. Mater.* **2018**, *28* (26), 1707550.
- (35) Marin, B. C.; Hsu, S.-W.; Chen, L.; Lo, A.; Zwissler, D. W.; Liu, Z.; Tao, A. R. Plasmon-Enhanced Two-Photon Absorption in Photoluminescent Semiconductor Nanocrystals. *ACS Photonics* **2016**, *3* (4), 526–531.
- (36) Lassiter, J. B.; Aizpurua, J.; Hernandez, L. I.; Brandl, D. W.; Romero, I.; Lal, S.; Hafner, J. H.; Nordlander, P.; Halas, N. J. Close Encounters between Two Nanoshells. *Nano Lett.* **2008**, *8* (4), 1212–1218.
- (37) Sun, G.; Khurgin, J. B. Comparative Study of Field Enhancement between Isolated and Coupled Metal Nanoparticles: An Analytical Approach. *Appl. Phys. Lett.* **2010**, *97* (26), 263110.
- (38) Ringler, M.; Schwemer, A.; Wunderlich, M.; Nichtl, A.; Kürzinger, K.; Klar, T. A.; Feldmann, J. Shaping Emission Spectra of Fluorescent Molecules with Single Plasmonic Nanoresonators. *Phys. Rev. Lett.* **2008**, *100* (20), 203002.
- (39) Humphrey, M. G.; Lockhart-Gillet, B.; Samoc, M.; Skelton, B. W.; Tolhurst, V.-A.; White, A. H.; Wilson, A. J.; Yates, B. F. Synthesis, Structure and Optical Limiting Properties of Organoruthenium-Chalcogenide Clusters. *J. Organomet. Chem.* **2005**, *690* (6), 1487–1497.
- (40) Roberts, R. L.; Schwich, T.; Corkery, T. C.; Cifuentes, M. P.; Green, K. A.; Farmer, J. D.; Low, P. J.; Marder, T. B.; Samoc, M.; Humphrey, M. G. Organometallic Complexes for Nonlinear Optics. 45. Dispersion of the Third-Order Nonlinear Optical Properties of Triphenylamine-Cored Alkynylruthenium Dendrimers. *Adv. Mater.* **2009**, *21* (22), 2318–2322.
- (41) Mertens, J.; Kleemann, M.-E.; Chikkaraddy, R.; Narang, P.; Baumberg, J. J. How Light Is Emitted by Plasmonic Metals. *Nano Lett.* **2017**, *17* (4), 2568–2574.
- (42) Inasawa, S.; Sugiyama, M.; Yamaguchi, Y. Laser-Induced Shape Transformation of Gold Nanoparticles below the Melting Point: The Effect of Surface Melting. *J. Phys. Chem. B* **2005**, *109* (8), 3104–3111.
- (43) de la Llave, E.; Herrera, S. E.; Méndez De Leo, L. P.; Williams, F. J. Molecular and Electronic Structure of Self-Assembled Monolayers Containing Ruthenium(II) Complexes on Gold Surfaces. *J. Phys. Chem. C* **2014**, *118* (37), 21420–21427.
- (44) Horton, M. J.; Ojambati, O. S.; Chikkaraddy, R.; Deacon, W. M.; Kongsuwan, N.; Demetriadou, A.; Hess, O.; Baumberg, J. J. Nanoscopy through a Plasmonic Nanolens. *Proc. Natl. Acad. Sci. U. S. A.* **2020**, *117* (5), 2275–2281.
- (45) Baumberg, J. J.; Aizpurua, J.; Mikkelsen, M. H.; Smith, D. R. Extreme Nanophotonics from Ultrathin Metallic Gaps. *Nat. Mater.* **2019**, *18*, 668.
- (46) Four, M.; Riehl, D.; Mongin, O.; Blanchard-Desce, M.; Lawson-Daku, L. M.; Moreau, J.; Chauvin, J.; Delaire, J. A.; Lemercier, G. A Novel Ruthenium(II) Complex for Two-Photon Absorption-Based Optical Power Limiting in the near-IR Range. *Phys. Chem. Chem. Phys.* **2011**, *13* (38), 17304–17312.
- (47) Gopinath, A.; Miyazono, E.; Faraon, A.; Rothmund, P. W. K. Engineering and Mapping Nanocavity Emission via Precision Placement of DNA Origami. *Nature* **2016**, *535* (7612), 401–405.
- (48) Chikkaraddy, R.; Turek, V. A.; Kongsuwan, N.; Benz, F.; Carnegie, C.; van de Goor, T.; de Nijs, B.; Demetriadou, A.; Hess, O.; Keyser, U. F.; Baumberg, J. J. Mapping Nanoscale Hotspots with Single-Molecule Emitters Assembled into Plasmonic Nanocavities Using DNA Origami. *Nano Lett.* **2018**, *18* (1), 405–411.
- (49) Ojambati, O. S.; Chikkaraddy, R.; Deacon, W. D.; Horton, M.; Kos, D.; Turek, V. A.; Keyser, U. F.; Baumberg, J. J. Quantum Electrodynamics at Room Temperature Coupling a Single Vibrating Molecule with a Plasmonic Nanocavity. *Nat. Commun.* **2019**, *10* (1), 1049.
- (50) Hübner, K.; Pilo-Pais, M.; Selbach, F.; Liedl, T.; Tinnefeld, P.; Stefani, F. D.; Acuna, G. P. Directing Single-Molecule Emission with DNA Origami-Assembled Optical Antennas. *Nano Lett.* **2019**, *19* (9), 6629–6634.
- (51) Scheibner, M.; Schmidt, T.; Worschech, L.; Forchel, A.; Bacher, G.; Passow, T.; Hommel, D. Superradiance of Quantum Dots. *Nat. Phys.* **2007**, *3* (2), 106–110.
- (52) Varguet, H.; Guérin, S.; Jauslin, H.; Colas des Francs, G. Cooperative Emission in Quantum Plasmonic Superradiance. *Phys. Rev. B: Condens. Matter Mater. Phys.* **2019**, *100* (4), 041115.
- (53) Jahnke, F.; Gies, C.; Aßmann, M.; Bayer, M.; Leymann, H. a. M.; Foerster, A.; Wiersig, J.; Schneider, C.; Kamp, M.; Höfling, S. Giant Photon Bunching, Superradiant Pulse Emission and Excitation Trapping in Quantum-Dot Nanolasers. *Nat. Commun.* **2016**, *7* (1), 1–7.
- (54) Li, B.; Lin, L.; Lin, H.; Wilson, B. C. Photosensitized Singlet Oxygen Generation and Detection: Recent Advances and Future Perspectives in Cancer Photodynamic Therapy. *J. Biophotonics* **2016**, *9* (11–12), 1314–1325.
- (55) Ojambati, O. S.; Deacon, W. M.; Chikkaraddy, R.; Readman, C.; Koczor-Benda, Z.; Rosta, E.; Scherman, O. A.; Baumberg, J. J. Breaking the Selection Rules of Spin-Forbidden Molecular Absorption in Plasmonic Nanocavities. *arXiv (Physics, Optics)*, May 11, 2020, arXiv:2005.05383; <https://arxiv.org/abs/2005.05383> (accessed 2020).
- (56) de Nijs, B.; Bowman, R. W.; Herrmann, L. O.; Benz, F.; Barrow, S. J.; Mertens, J.; Sigle, D. O.; Chikkaraddy, R.; Eiden, A.; Ferrari, A.; Scherman, O. A.; Baumberg, J. J. Unfolding the Contents of Sub-Nm Plasmonic Gaps Using Normalising Plasmon Resonance Spectroscopy. *Faraday Discuss.* **2015**, *178*, 185–193.
- (57) Benz, F.; de Nijs, B.; Tserkezis, C.; Chikkaraddy, R.; Sigle, D. O.; Pukenas, L.; Evans, S. D.; Aizpurua, J.; Baumberg, J. J. Generalized Circuit Model for Coupled Plasmonic Systems. *Opt. Express* **2015**, *23* (26), 33255.
- (58) Kleemann, M.-E.; Mertens, J.; Zheng, X.; Cormier, S.; Turek, V.; Benz, F.; Chikkaraddy, R.; Deacon, W.; Lombardi, A.; Moshchalkov, V. V.; Vandenbosch, G. A. E.; Baumberg, J. J. Revealing Nanostructures through Plasmon Polarimetry. *ACS Nano* **2017**, *11*, 850.